Supporting Information

Nichols et al. 10.1073/pnas.1208881109

SI Materials and Methods

Rhodamine-Labeled 2fAP in Airway Epithelium. Tetramethyl-rhodamine conjugated to the C-terminal ornithine residue of either 2fAP (Rh-2fAP) was synthesized by Genemed. Naïve WT and $PAR_2^{-/-}$ mice were administered Rho-2fAP intranasally for 0, 2, and 24 h after which mice were killed and pulmonary lobes were extracted and flash frozen in OCT. Five-micrometer sections were cut with Microm HM500 OMV Motorized Cryostat and were fixed with 4% (wt/vol) PFA for 20 min and blocked and permeabilized with goat serum (2 × 5 min). Sections incubated with 200 ng/mL Lung Surfactant Protein antibody (Neomarkers; ms-704-PO). Sections were washed with PBS+Tween 20 [0.05% (vol/vol)] and stained with secondary antibody (Gt-anti-Mo 530abs) diluted 1:500 in PBS for 40 min in dark at room temperature. Nuclei were stained with TOPRO-3 (1:1,000) for 20 min. Sections were mounted with V mounting media and imaged with Zeiss 510 confocal microscope.

Lung Digest Preparations. Lung single-cell suspension obtained by incubating lung samples with glass beads and collagenase 3 at 37 °C for 60 min, shaking them every 7 min during the incubation. Red blood cells were lysed with ammonium chloride, and samples were prepared for flow cytometry.

Adoptive Transfer. To allow easy identification of transplanted cells, donor mice were crossed with GFP mice so that the transplanted cells were GFP positive (genotypes: $GFP^{+/-}PAR2^{-/-}$ and $GFP^{+/-}PAR2^{+/+}$).

Smooth Muscle Relaxation. Primary first-order mouse bronchiolar rings with intact epithelium were, and 2 mm segments were mounted in a myograph at resting tension, in a 37 °C Krebs buffer bath. After 60 min of equilibration at ∼0.5 g of resting tension, tissues were tested treated with 50 mM KCl (tests responsiveness), washed, and precontracted with 500 nM carbachol. After stable force was achieved (100% on the waveforms in response to carbachol), tissues were treated with increasing concentrations of 2fAP or CP, and the relaxation response was recorded. Relaxation was expressed as a percentage reduction in tension (%) relative to the tension measured in the presence of carbachol.

AHR Measurements. Airway hyperresponsiveness was measured as described previously (1). In brief, lung mechanics was measured in anesthetized (i.p. 65 mg/kg sodium pentobarbital), paralyzed (0.25 mg/kg pancuronium bromide), and tracheotomized mice 24 h after the last OVA challenge. The forced oscillation technique was used, using a 3-s optimized pseudorandom signal containing frequencies ranging from 0.25 to 19.63 Hz. Mice were ventilated with 100% oxygen at 150 breaths per minute at a constant volume of 8 mL/kg with a positive end-expiratory pressure of 3 cmH_2O, using a computer-controlled small animal ventilator (flexiVent; SCIREQ). The cardiovascular function of the mice was inferred from heart rate data acquired using EKG electrodes and transmitted via loudspeaker. Following ∼5 min of regular ventilation, a standard lung volume history was established followed by the acquisition of three baseline respiratory input impedance measurements. Bronchospasm was induced by jugular vein administration of increasing doses of MCh (25, 50, 100 μg/kg), and the impedance measurements were made every 12 s and averaged over 2 min. A 5-min washout period was included between each MCh challenge that included two deep inspirations. The resultant total lung impedance signal contains information about the resistance and elastance properties of the lung from which Newtonian resistance was calculated using the constant-phase model. In an idealized lung model, Newtonian resistance is a good indicator of the luminal diameter of the conducting airways.

Buffer Compositions. For smooth muscle relaxation assay, Krebs buffer (pH 7.4) consists of the following (in mmol/L): NaCl, 120; $NaHCO_3$, 25; KCl, 4.8; NaH_2PO_4, 1.2; dextrose, 11.0; and $CaCl_2$, 1.8, aerated with 95% O_2 and 5% CO_2.

FACS buffer consists of the following: 1% BSA and 0.1 mM EDTA in PBS.

Flow Cytometry Gating Strategy. Other cells (which presumably includes alveolar macrophages and dendritic cells) were not further characterized. Group A received conjugated antibodies against CD11c, CCR3, CD45, GR1, CD11b, and CD3. Group B received conjugated antibodies against CD11c, CD19, CD8, CD4, CD11b, and F480 (all antibodies were from eBioscience). Cells were washed and analyzed with BD FACSCANTO II flow cytometer and FlowJo analysis software, version 8.7.3. Isolated lung tissue samples were analyzed with an identical protocol. For quantification by flow cytometry, cells were gated as follows: $CD45^+$ cells were selected, and live granulocytes and lymphocytes were identified by forward versus side scatter (FSC vs. SSC). For Group A (antibodies to CD11c, CCR3, CD45, GR1, CD11b, and CD3), from the $CD45^+$ gate, low side scatter cells were scored as lymphocytes (L*), $CD11b^-/CD3^+$ cells were scored as T lymphocytes (L*). From the $CD45^+$/high side scatter gate, populations that were $CD11b^+/CCR3^+/GR1^-$ were scored as eosinophils. Cells that were $CD11b^+/GR1^+$ were scored as neutrophils. To identify specific populations of lymphocytes, Group B samples (antibodies to CD11c, CD19, CD8, CD4, CD11b, and F480) were used and low SSC cells were scored as $CD4^+/CD8^-$ (T helper), $CD8^+/CD4^-$ (cytotoxic T cells), and $CD19^+$ (B cells).

Histological Scoring. H&E-stained lung samples were scored for presence of cellular inflammation and perivascular infiltration as follows: 0, no inflammatory cells present in epithelial or perivascular tissue; 1, scattered inflammatory cells present in epithelium and around vessels, with no thickening of the vessel wall; 2, many inflammatory cells present in epithelium with one to two rings of cells around vessels; 3, 100+ inflammatory cells found in clusters throughout epithelium with three or more rings of cells around vessels; 4, nearly continuous layer of inflammatory cells extending from vasculature throughout epithelium, loss of distinction between perivascular and epithelial tissue.

1. Lin R, et al. (2012) Chronic treatment in vivo with β-adrenoceptor agonists induces dysfunction of airway β_2-adrenoceptors and exacerbates lung inflammation in mice. *Br J Pharmacol* 165:2365–2377.

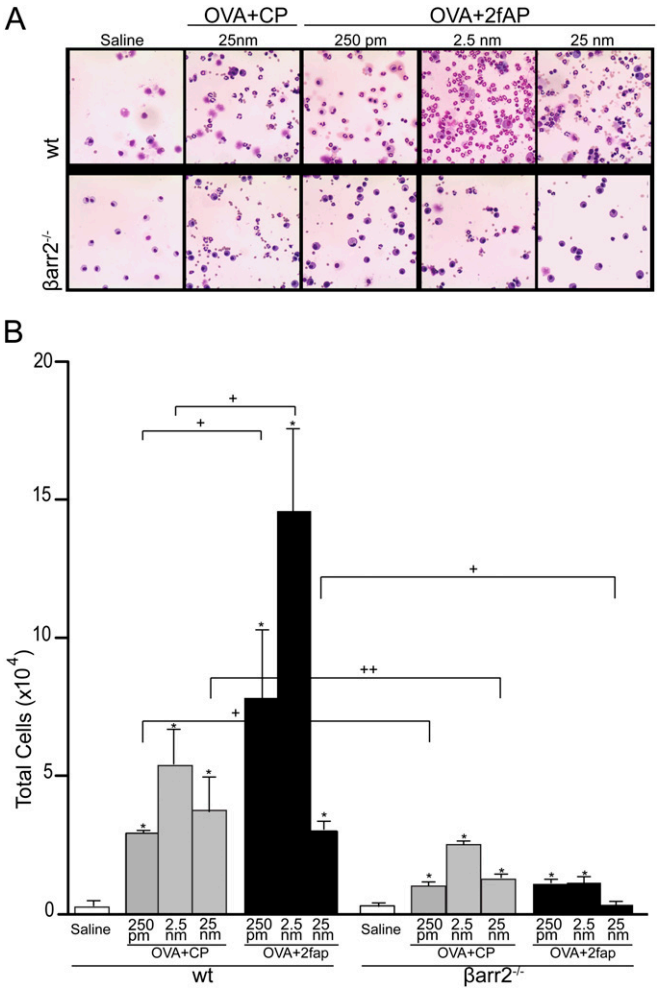

Fig. S1. Dose-dependent augmentation of OVA-induced asthma by 2fAP. WT and β-arrestin-2$^{-/-}$ mice were given an i.p. injection of OVA+alum on days 1 and 6 followed by two intranasal challenges on days 12 and 14 containing OVA+ increasing doses (250 pmol, 2.5 nmol, or 25 nmol) of PAR_2-activating peptide (2fAP) or a negative control peptide (CP). As a negative control for OVA-induced inflammation, mice were given saline in place of both the i.p. sensitization and intranasal challenges. The schematic for this experiment is depicted in Fig. 1*A* of the main text. On day 15, BALF was collected for analysis of leukocyte infiltration. (*A*) Representative cytospins of BALF cells collected from saline-treated controls, OVA+CP (25 nmol), and OVA+2fAP (all three concentrations) shows increased eosinophils and lymphocytes in WT mice receiving 2.5 and 25 nmol of 2fAP during the challenge phase. Maximal inflammatory cell recruitment was observed with 2.5 nmol of 2fAP. (*B*) Total cell count of BALF cells reveals that 25 nmol of 2fAP administered during the challenge phase gives the maximal augmentation of cell recruitment to the BALF. A statistically significant increase is observed with 2.5 nmol and no significant increase in cells is observed with 25 nmol. For all subsequent studies, 2.5 nmol of 2fAP is the amount used in the challenges. * ($P > 0.05$) illustrates statistical significance from saline-treated controls. $^{+}P > 0.05$ and $^{++}P > 0.01$ above brackets demonstrate significant difference between OVA-treated groups.

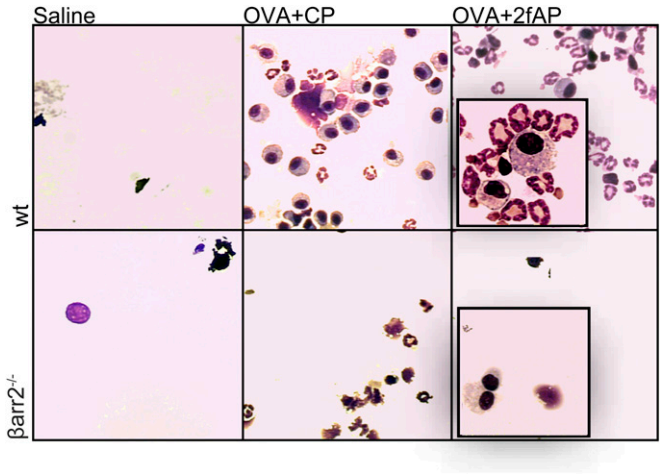

Fig. S2. Representative cytospin images of BAL fluid. Images illustrate increase in inflammatory cells recruited to lungs in WT mice challenged with OVA+2fAP. Of equal importance is the augmented recruitment of eosinophils, an indicator of allergic disease, in the aforementioned mice (see zoom inlay). Note the reduced total cell number and absence of eosinophils in β-arrestin-$2^{-/-}$ mice also challenged with OVA+2fAP (see zoom inlay).

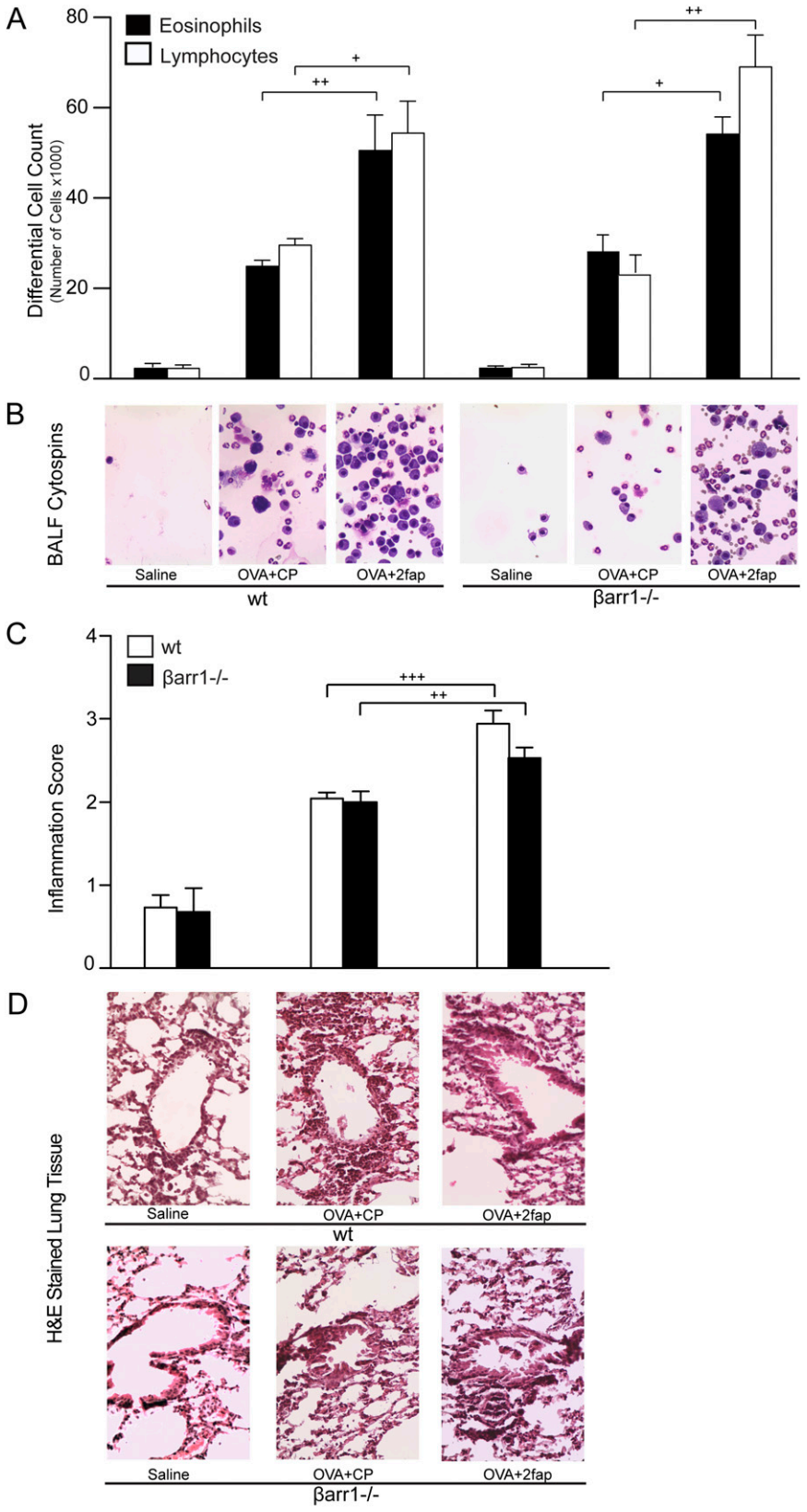

Fig. S3. OVA-induced and 2fAP-augmented inflammation is independent of β-arrestin-1. The same model of airway inflammation was run in WT versus β-arrestin-1 mice (4 mice per treatment, 24 mice total), and both BALF cell distribution and lung histology were examined. (*A*) Bar graph of eosinophils and lymphocytes found in BALF, determined from differential count of cytospin images. Differential cell determined in 10 different images from each mouse. Both the moderate increase in eosinophil and lymphocyte recruitment observed with OVA+CP and the augmented recruitment observed in the mice receiving 2fAP were maintained in the β-arrestin-1$^{-/-}$ mice, indicating that both are independent of β-arrestin-1. (*B*) Representative cytospins of BALF from each experimental condition are shown. (*C*) Histological scoring was performed on a 0–4 scale, as described for Fig. 1, where 0 represents no inflammation and 4 represents a high

Legend continued on following page

level of inflammation with multiple rings of immune cells around the peribronchial region that form a continuum with the airway epithelium. (*D*) H&E-stained sections of lungs from each experimental condition are shown, demonstrating 2fAP-induced inflammation in both WT and β-arrestin-1$^{-/-}$ mice. Once again, the inflammation induced by 2fAP is maintained in the β-arrestin-1$^{-/-}$ mice. All treatment group significantly different from saline-treated controls ($P > 0.005$). $^{+}P > 0.05$, $^{++}P > 0.01$, and $^{+++}P > 0.001$ above brackets demonstrates significant difference between OVA-treated groups.

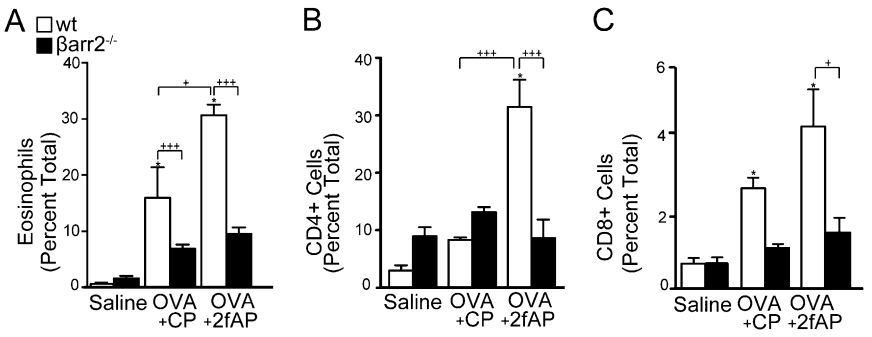

Fig. S4. Eosinophil, CD4^{+} and CD8^{+} lymphocytes are reduced in lung tissue of β-arrestin-2$^{-/-}$ mice. Lung digests were prepared from mice treated as described in Fig. 1*A*, and cells were stained with antibodies to specific cell surface markers and analyzed by flow cytometer to identify populations of eosinophils (*A*), CD4^{+} T-cells (*B*), and (*C*) CD8^{-} T-cells. Gating strategies were the same as for BALF samples mentioned in *Materials and Methods*. $^{*}P > 0.05$ illustrates statistical significance from saline-treated controls. $^{+}P > 0.05$ and $^{+++}P > 0.001$ above brackets demonstrate significantdifference between OVA-treated groups.

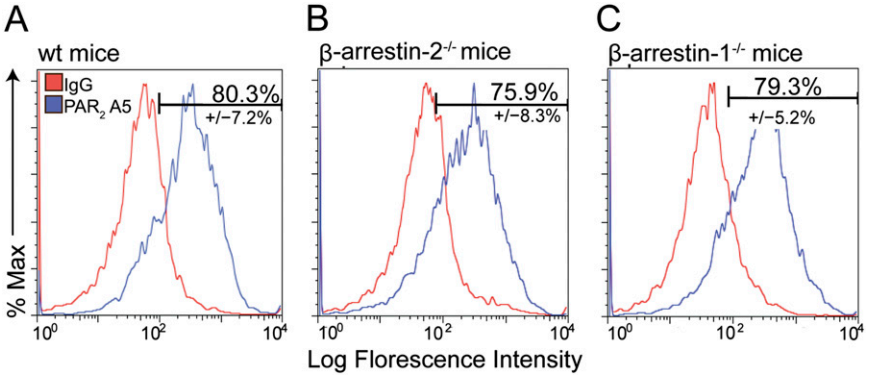

Fig. S5. PAR_2 expression is not altered in β-arrestin knockout mice. Lungs and associated first-order bronchioles from WT, β-arrestin-1$^{-/-}$, and β-arrestin-2$^{-/-}$ mice were digested and prepared as described for Fig. S4. Cells were divided into two aliquots, one set was labeled with rabbit IgG (negative control) and the other with an antibody to the extracellular N terminus of PAR_2 (A5, polyclonal antisera raised against the mouse PAR2 sequence: PNSKGRSLIGRLDTP, encompassing the cleavage site and tethered ligand region). This antibody has been used to identify PAR_2 in primary tissues and cells and is similar to B5 antibody used to identify PAR2 in earlier studies (1). After 1 h on ice, cells were washed, and Alexa 488-conjugated secondary antibody was added for 1 h. Cells were again washed and resuspended in FACS buffer, and live cells were analyzed for the presence of surface receptor. Shown are overlays of histograms for IgG in red (negative control) and A5 (PAR2) in blue for WT (*A*), β-arrestin-1$^{-/-}$ (*B*), and β-arrestin-2$^{-/-}$ (*C*) mice.

1. Brown JK, Hollenberg MD, Jones CA (2006) Tryptase activates phosphatidylinositol 3-kinases proteolytically independently from proteinase-activated receptor-2 in cultured dog airway smooth muscle cells. *Am J Physiol Lung Cell Mol Physiol* 290:L259–L269.

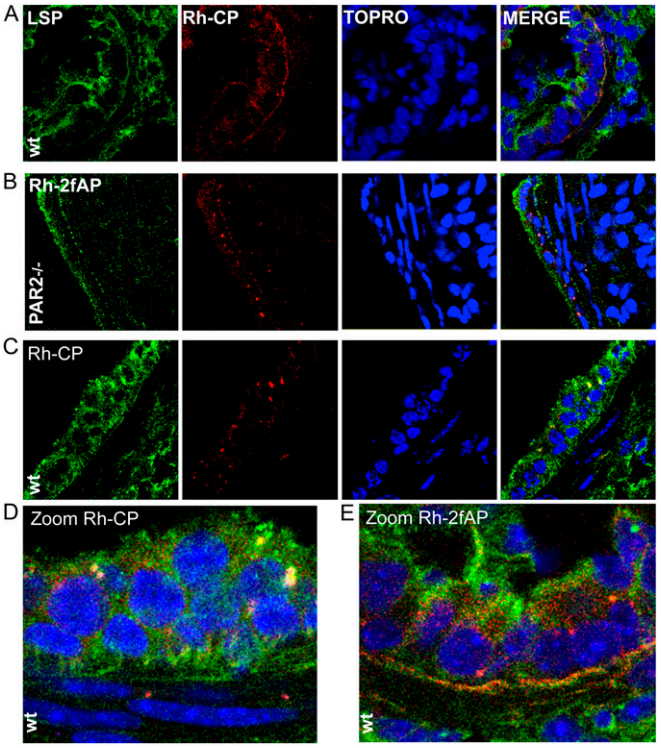

Fig. S6. Intranasally administered PAR_2 activating peptide can access the basolateral side of the airways. WT and $PAR_2^{-/-}$ mice were given rhodamine-labeled 2fAP (Rh-2fAP), or rhodamine-labeled control peptide (Rh-CP), intranasally, and lungs were harvested 2 h after administration. Frozen sections were stained with lung surfactant protein (LSP) (in green) and TOPRO 3 to visualize nuclei (in blue) and then imaged by confocal microscopy using a Zeiss LSM510, 100× objective. Representative images showing Rh-2fAP labeling (red) throughout the airway epithelium and serosa in WT (*A*) but not $PAR_2^{-/-}$ mice (*B*) or WT mice given Rh-CP (*C*) are shown. Zoomed images (3×) of Rh-CP-treated WT (*D*) and Rh-2fAP-treated WT (*E*) lungs are shown.

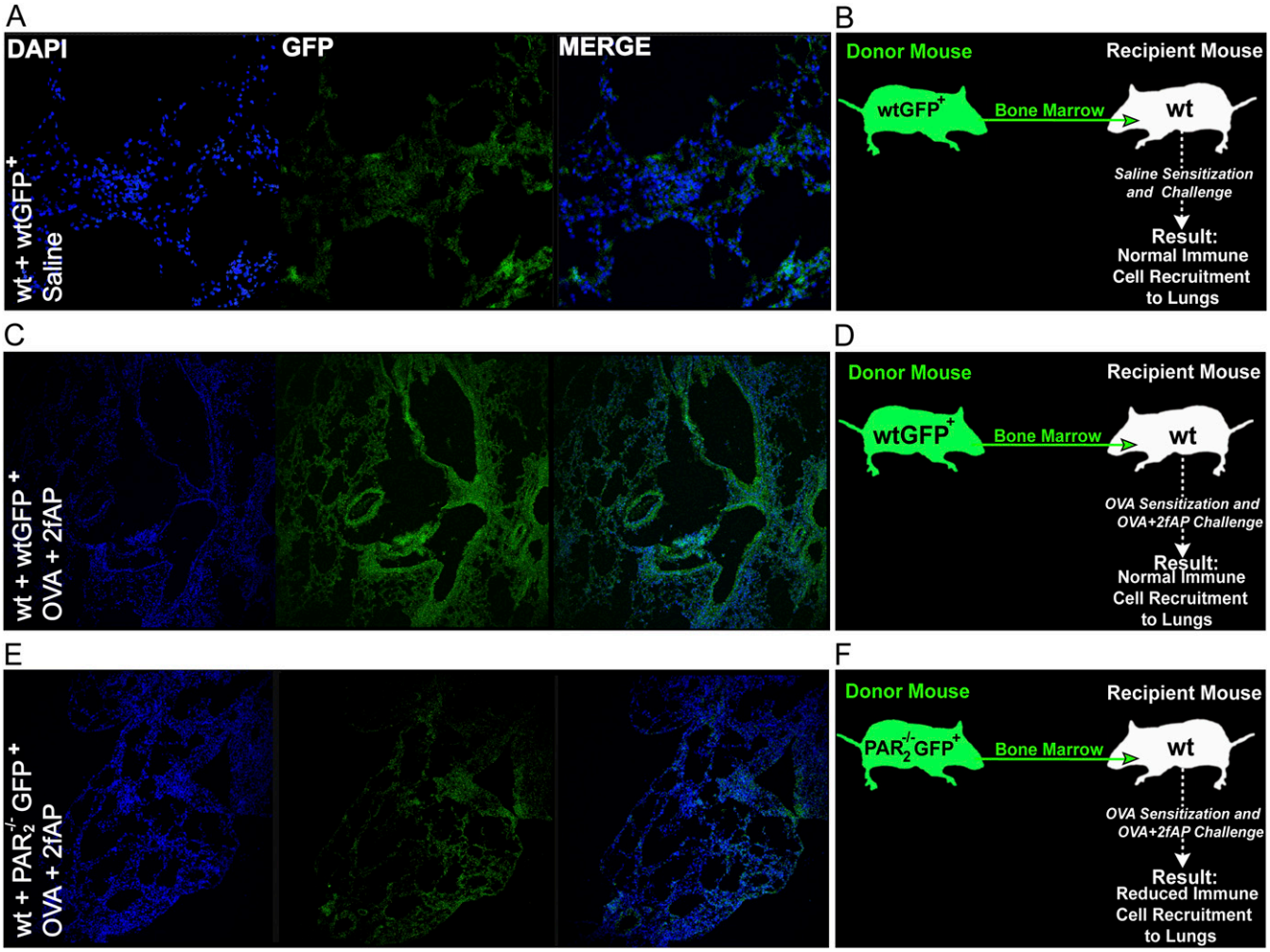

Fig. S7. Adoptive transfer of wtGFP$^+$ hematopoietic cells restores normal inflammatory response. (*A*) wtGFP$^+$ mice saline-treated have little inflammation in perivascular or peribronchial regions. (*B*) Cartoon illustration of adoptive transfer protocol identifying donor and recipient. (*C* and *D*) WT recipients of wtGFP$^+$ hematopoietic cells and challenged with OVA+2fAP show increased inflammation in the region of interest. (*E* and *F*) WT recipients of $PAR_2^{-/-}$/GFP$^+$ hematopoietic cells show little inflammation even after OVA+2fAP treatment.

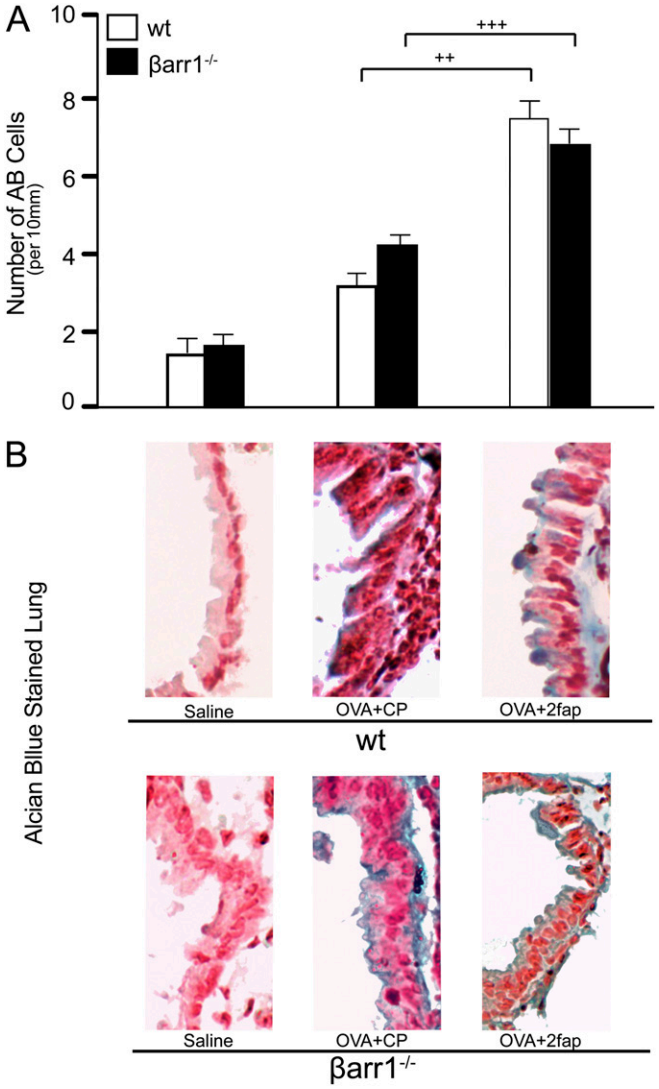

Fig. S8. Mucin production induced by PAR_2 is independent of β-arrestin-1. WT and β-arrestin-$1^{-/-}$ mice from the experiment described in Fig. S3 were stained with Alcian blue (as described in Fig. 5), and the number of mucin-producing cells per 10 mm was determined using Adobe Photoshop. (*A*) Quantification of mucus-producing cells. (*B*) Representative images of Alcian blue-stained airways. All treatment groups were significantly different from saline-treated controls ($P > 0.005$). $^{++}P > 0.01$ and $^{+++}P > 0.001$ above brackets demonstrate difference between OVA-treated groups.